Iterative Tomographic Image Reconstruction Using Nonuniform Fast Fourier Transforms

Jeffrey A. Fessler[*]

4240 EECS, The University of Michigan, Ann Arbor, MI 48109-2122
`fessler@umich.edu`

April 16, 2002

ABSTRACT

Fourier-based reprojection methods have the potential to reduce the computation time in iterative tomographic image reconstruction. Interpolation errors are a limitation of Fourier-based reprojection methods. We apply a min-max interpolation method for the nonuniform fast Fourier transform (NUFFT) to minimize the interpolation errors. Numerical results show that the min-max NUFFT approach provides substantially lower approximation errors in tomographic reprojection and backprojection than conventional interpolation methods.

Keywords: *Nonuniform FFT, min-max interpolation, tomography*

I. INTRODUCTION

Iterative methods for tomographic image reconstruction offer numerous advantages over the conventional filtered backprojection method. The late 1990's saw commercial release of 2D iterative reconstruction methods for PET and SPECT systems. The computation burden of forward and backprojection operations remains the primary hindrance to wider use of iterative methods for fully 3D image reconstruction. This paper describes a new efficient approach to forward and backprojection using a combination of the Fourier-slice theorem and a min-max method for the nonuniform fast Fourier transform. This approach is particularly well suited to the geometries of PET scanners.

For most iterative reconstruction methods, each iteration requires computation of one "forward projection" and one "backprojection," where the forward projection is roughly a discretized evaluation of the Radon transform, and the backprojector is the adjoint of the forward projector. The projection and backprojection steps traditionally involve operations such as computing the lengths of intersections between each tomographic ray and each image voxel. These operations are the principal computational bottleneck in iterative reconstruction methods, particularly in 3D image reconstruction. A variety of methods for accelerating this process have been proposed, see *e.g.*, [1].

One natural approach to forward projection is to use the Fourier-slice theorem [2, p. 56]. This theorem relates the 1D FT of each projection to samples of the 2D FT of the object on a polar grid[1]. The use of the Fourier-slice theorem as a tool for *reprojection* was noted in the late 1980's by Crawford *et al.* [3, 4], in the context of correction of beam hardening in X-ray CT, and by Stearns *et al.* [5, 6], in the context of filling in missing projections in (noniterative) 3D PET image reconstruction. These approaches were apparently largely abandoned thereafter due in part to unacceptable image artifacts caused by the large interpolation errors associated with conventional "gridding" methods for converting between polar and Cartesian coordinates in frequency space. The importance of accurate interpolation for gridding has been analyzed rigorously [7, p. 119]. We propose to apply our min-max approach to the nonuniform fast Fourier transform (NUFFT) [8–11] to this problem, thereby largely eliminating those artifacts and perhaps helping salvage the utility of Fourier-based reprojection.

More recently, Delaney and Bresler [12] proposed a clever iterative algorithm that uses Fourier principles to combine projection and backprojection into a single filtering operation that is efficiently implemented with a fast Fourier transform (FFT) algorithm. However, that formulation is restricted to a particular type of weighting matrix (block-circulant) that is suboptimal for data with nonstationary statistics, such as low-count PET scans. The proposed NUFFT-based projector allows us to use weighting matrices of the form needed in PET [13], albeit at the ex-

[1]Shift-invariant detector blur is easily included in this framework.

pense of greater computation than required by the algorithm in [12]. We suspect that the Delaney and Bresler algorithm would be very useful for quickly forming an initial image estimate for subsequent iterations by another algorithm based on statistical weighting.

Very recently, Matej *et al.* have applied Fourier-based reprojection [14] for (noniterative) fully 3D PET reconstruction and [15] for calculation of attenuation correction factors in PET. They used Kaiser-Bessel windows for interpolation, which are known to be reasonably accurate [16,17] but without explicitly evaluating the accuracy.

The concepts in this paper are somewhat related to "gridding" methods for interpolation in frequency space. Such methods have been considered both for tomography and for general applications, *e.g.*, [5, 16–43], and for MR imaging [44–49]. In most of these papers, the focus was using gridding to find a *non-iterative* approximate solution to an *inverse* problem. In contrast, we use Fourier-based reprojection as a tool for calculating the *forward* problem, and allow an iterative reconstruction methods to solve the inverse problem. The optimality claims we make are for the forward problem only. The prospect of using graphics hardware to assist in this projection process is enticing [50–54].

To our knowledge, the work herein and presented in [8] represents the first application of a NUFFT method to iterative tomographic image reconstruction. Potts *et al.* have applied the NUFFT to direct Fourier reconstruction using truncated gaussian bell as the interpolation kernel [42,43]. (A similar approach was described by Tabei and Ueda without the NUFFT moniker [32].) That method is undoubtably very good, but no claims of optimality can be made. Our min-max method is optimal for the NUFFT need for reprojection, but we make no claim of optimality of our min-max interpolator for the direct Fourier reconstruction method. We conjecture that a min-max approach could be devised for the direct Fourier reconstruction method [39].

Section II reviews the min-max NUFFT method. Section III describes the application of the NUFFT method to reprojection. Section IV gives numerical results.

II. NUFFT IN 2D

The section reviews the NUFFT method presented in [11]. We focus on the 2D case since [11] emphasized only the 1D case. The extension to 3D is straightforward.

A. Problem statement

We are given a 2D finite-extent signal $x[n_1, n_2]$, $n_1 = 0, \ldots, N_1 - 1$, $n_2 = 0, \ldots, N_2 - 1$, and we want to evaluate its (discrete space) Fourier transform (DSFT):

$$X(\omega_1, \omega_2) = \sum_{n_1=0}^{N_1-1} \sum_{n_2=0}^{N_2-1} x[n_1, n_2] e^{-\imath(\omega_1 n_1 + \omega_2 n_2)}$$

at a finite collection of (nonuniformly spaced) frequency locations $\{(\omega_{1,m}, \omega_{2,m}) : m = 1, \ldots, M\}$.

The NUFFT approach is to first compute an oversampled, weighted 2D FFT of $x[n_1, n_2]$, and then interpolate the DFT coefficients onto the desired frequency locations.

The first step is to choose convenient $K_1 \geq N_1$ and $K_2 \geq N_2$ and compute a weighted K_1, K_2-point DFT:

$$Y[k_1, k_2] = \\ \sum_{n_1=0}^{N_1-1} \sum_{n_2=0}^{N_2-1} s[n_1, n_2] x[n_1, n_2] e^{-\imath(\gamma_1 k_1 n_1 + \gamma_2 k_2 n_2)}$$

for $k_1 = 0, \ldots, K_1$ and $k_2 = 0, \ldots, K_2$, using the 2D FFT algorithm, where $\gamma_1 \triangleq 2\pi/K_1$ and $\gamma_2 \triangleq 2\pi/K_2$. The nonzero $s[n_1, n_2]$'s are called *scaling factors* and are designed to partially compensate for imperfections in the subsequent interpolation step. Their choice strongly affects the accuracy of the method [11]. For simplicity, we consider only *separable* scaling factors of the form

$$s[n_1, n_2] = s_1[n_1] s_2[n_2].$$

Furthermore, we assume that $s_1[n_1]$ has a low-order Fourier-series representation [11] of the form

$$s_1[n_1] = \sum_{t=-L_1}^{L_1} \alpha_t e^{\imath \gamma_1 \beta_1 (n_1 - \eta_1)},$$

where the coefficients are Hermitian symmetric, the fundamental frequency scaling β_1 is a design variable, and $\eta_1 \triangleq (N_1 - 1)/2$. Good values for β_1 and the $\alpha'_t s$ are tabulated in [11]. A similar expansion holds for $s_2[n_2]$.

This first step requires $O(K_1 K_2 \log_2 K_1 K_2)$ operations, which can be reduced to $O(K_1 K_2 \log_2 N_1 N_2)$ if one applies a reduced FFT [11]. Of course

$$Y[k_1, k_2] = Y(\omega_1, \omega_2)\Big|_{\omega_1 = \gamma_1 k_1, \, \omega_2 = \gamma_2 k_2},$$

where $Y(\omega_1, \omega_2)$ denotes the FT of the modified signal $y[n_1, n_2] = x[n_1, n_2] s[n_1, n_2]$, so the DFT provides samples of $Y(\omega_1, \omega_2)$ on the set

$$\Omega \triangleq \{(\omega_1, \omega_2) : \omega_1 = \gamma_1 k_1, \, \omega_2 = \gamma_2 k_2, \\ k_1 = 0, \ldots, K_1 - 1, \, k_2 = 0, \ldots, K_2 - 1\}.$$

The second step is to choose a local $J_1 \times J_2$ neighborhood within Ω around each frequency location of interest

$\omega_{1,m}, \omega_{2,m}$, and estimate $X(\omega_{1,m}, \omega_{2,m})$ by linearly interpolating the corresponding $X[k_1, k_2]$ values. To express the interpolator mathematically, define the following integer offset:

$$o_1(\omega) \triangleq \begin{cases} \left(\arg\min_{k\in\mathbb{Z}} |\omega - \gamma_1 k|\right) - \dfrac{J_1+1}{2}, & J_1 \text{ odd} \\[2ex] (\max\{k \in \mathbb{Z} : \omega \geq \gamma_1 k\}) - \dfrac{J_1}{2}, & J_1 \text{ even,} \end{cases} \tag{1}$$

likewise for $o_2(\omega)$. Then the min-max interpolator derived in [11] turns out to have the following separable form:

$$\hat{X}(\omega_1, \omega_2) = \sum_{j_1=1}^{J_1} \sum_{j_2=1}^{J_2}$$
$$u_{j_1}^\star(\omega_1, N_1, J_1, K_1)\, u_{j_2}^\star(\omega_2, N_2, J_2, K_2)$$
$$\cdot Y\left[\{o_1(\omega_1) + j_1\}_{K_1}, \{o_2(\omega_2) + j_2\}_{K_1}\right]$$

where $\{\cdot\}_K$ denotes the modulo-K operation (ensuring that $\hat{X}$ is 2π-periodic), and "$\star$" denotes complex conjugate.

As derived in [11], the interpolation kernel itself has the following form:

$$u_1(\omega) = \Lambda_1'(\omega) T_1 r_1(\omega)$$

where $\Lambda_1(\omega)$ is a diagonal matrix with elements

$$[\Lambda_1(\omega)]_{jj} = e^{-i[\omega - \gamma_1(o_1(\omega)+j))]\eta_1},$$

"$'$" denotes Hermitian transpose, T_1 is a $J_1 \times J_1$ matrix with elements

$$[T_1^{-1}]_{l,j} = \sum_{t=-L_1}^{L_1} \sum_{s=-L_1}^{L_1} \alpha_t \alpha_s^\star \operatorname{sinc}\left(\frac{j - l + \beta_1(t - s)}{K_1/N_1}\right),$$

where $\operatorname{sinc}(t) \triangleq \sin(\pi t)/(\pi t)$, and r_1 is a J_1-vector with elements

$$[r_1]_j = \sum_{t=-L_1}^{L_1} \alpha_t \operatorname{sinc}\left(\frac{\omega/\gamma_1 - o_1(\omega) - j + \beta_1 t}{K_1/N_1}\right).$$

We similarly define u_2, Λ_2, T_2, and r_2.

Mathematically, for a given choice of K_1, K_2, J_1, J_2 and $s[n_1, n_2]$, the interpolator described above minimizes the worst-case approximation error $\left|\hat{X}(\omega_1, \omega_2) - X(\omega_1, \omega_2)\right|$ over all signals $x[n_1, n_2]$ with unit norm. The rough intuition is that the vector r is the standard truncated sinc interpolator, the matrix R optimally compensates for the truncation, and the Λ provides the usual linear phase associated with frequency-space interpolation.

Matlab subroutines for evaluating the above quantities are available online[2]. To minimize computation time per iteration, we precompute and store all of the offsets $\{(o_1(\omega_1), o_2(\omega_2))\}$ and interpolation coefficients $\{u_1(\omega_1), u_1(\omega_2)\}$ for the relevant $(\omega_{1,m}, \omega_{2,m})$'s prior to iterating.

III. TOMOGRAPHIC REPROJECTION

This section reviews reprojection starting with the continuous case and then working towards the discrete case relevant for iterative image reconstruction and for which the NUFFT is applicable.

Let $g(x, y)$ denote the 2D image whose projections we wish to compute, and assume that $g(x, y) \overset{\mathcal{F}_2}{\longleftrightarrow} G(f_X, f_Y)$ where

$$G(f_X, f_Y) = \iint g(x, y)\, e^{-i2\pi(xf_X + yf_Y)}\, dx\, dy.$$

In polar coordinates:

$$G_\theta(\rho) = G(\rho\cos\theta, \rho\sin\theta),$$

and since $g(x, y)$ is real, $G_\theta^\star(\rho) = G_\theta(-\rho)$.

By the Fourier-slice theorem [2, p. 56], the projection at angle θ as a function of radial distance r is given by:

$$p_\theta(r) = \int_{L(r,\theta)} g(x, y)\, dl = \int G_\theta(\rho)\, e^{i2\pi\rho r}\, d\rho,$$

where $L(r, \theta)$ denotes the line at angle θ taken counterclockwise from the y axis, at distance r from the origin.

A classical sinogram model would consist of samples of $p_\theta(r)$, but that approach ignores the detector blur of the imaging system. Assume that the detector response is simply shift-invariant radial blur with impulse response $h(r)$ and corresponding frequency response $H(f)$. Accounting for the center of rotation of the imaging system, the detector sampling distance Δ_r, and the detector blur, we wish to compute

$$\begin{aligned} y_\theta[n] &= \left. (p_\theta(r) * h(r))\right|_{r=(n-\eta_r)\Delta_r} \tag{2} \\ &= \int G_\theta(\rho)\, H(\rho) e^{i2\pi\rho\Delta_r(n-\eta_r)}\, d\rho \\ &= \int_{-\infty}^{\infty} Y_\theta(\rho) e^{i2\pi\rho\Delta_r n}\, d\rho, \tag{3} \end{aligned}$$

for $n = 0, \ldots, N_r - 1$, where N_r is the number of radial samples, and

$$Y_\theta(\rho) \triangleq G_\theta(\rho)\, H(\rho) e^{-i2\pi\rho\Delta_r\eta_r}. \tag{4}$$

Typically $\eta_{\mathrm{r}} = (N_{\mathrm{r}} - 1)/2$.

For a forward projection, we must compute approximations to (3) for a finite collection of θ's. For speed, we want to approximate (3) using an K-point inverse FFT, where we may choose any convenient $K \geq N_{\mathrm{r}}$. Define $\delta = 1/(K\Delta_{\mathrm{r}})$. Then the natural discretization of (3) is

$$
\begin{aligned}
y_\theta[n] &\approx \sum_{k=-K/2}^{K/2-1} \delta Y_\theta(k\delta) e^{\imath 2\pi(k\delta)\Delta_{\mathrm{r}} n} \\
&= \frac{1}{K} \sum_{k=-K/2}^{K/2-1} Z_\theta[k] e^{\imath \gamma k n}, \quad\quad (5)
\end{aligned}
$$

where $\gamma \triangleq 2\pi/K$ and

$$
Z_\theta[k] \triangleq \frac{1}{\Delta_{\mathrm{r}}} Y_\theta(k\delta). \quad\quad (6)
$$

The summation (5) is precisely a K-point inverse FFT.

Thus, given samples $Z_\theta[k]$ of the spectrum $Y_\theta(\rho)$ (or approximations thereof), we can determine $y_\theta[n]$ by a simple scaled inverse FFT. To compute those samples $Z_\theta[k]$, we apply the 2D NUFFT method.

A. Discretizing the 2D FT

In the practice of iterative image reconstruction, rather than operating on a continuous object $g(x, y)$, we want to forward project a discretized object such as the following:

$$
g(x, y) = \sum_{n_1=0}^{N_1-1} \sum_{n_2=0}^{N_2-1} g[n_1, n_2] b(x - n_1\Delta_1, y - n_2\Delta_2),
$$

$$ (7) $$

which has corresponding spectrum

$$
G(f_{\mathrm{X}}, f_{\mathrm{Y}}) = B(f_{\mathrm{X}}, f_{\mathrm{Y}}) G_d(2\pi f_{\mathrm{X}}\Delta_1, 2\pi f_{\mathrm{Y}}\Delta_2) \quad (8)
$$

where $B(f_{\mathrm{X}}, f_{\mathrm{Y}})$ is the 2D FT of the basis function $b(x, y)$, and the 2D FT of $g[n_1, n_2]$ is:

$$
G_d(\omega_1, \omega_2) = \sum_{n_1=0}^{N_1-1} \sum_{n_2=0}^{N_2-1} g[n_1, n_2] e^{-\imath(\omega_1 n_1 + \omega_2 n_2)}. \quad (9)
$$

Combining (4) and (8) yields

$$
\begin{aligned}
Y_\theta(\rho) &= B(\rho\cos\theta, \rho\sin\theta) \, H(\rho) \, e^{-\imath 2\pi\rho\Delta_{\mathrm{r}}\eta_{\mathrm{r}}} \\
&\quad \cdot G_d(2\pi\Delta_1\rho\cos\theta, \, 2\pi\Delta_2\rho\sin\theta) \quad (10)
\end{aligned}
$$

These relationships suggest the following approach to forward projection.

Step 1. Use the 2D NUFFT method with $\omega_1 = 2\pi f_{\mathrm{X}}\Delta_1$ and $\omega_2 = 2\pi f_{\mathrm{X}}\Delta_2$ to compute an accurate approximation to the double summation in (9). Use $f_{\mathrm{X}} =$

$\rho\cos\theta$ and $f_{\mathrm{Y}} = \rho\sin\theta$ with $\rho = k/(K\Delta_{\mathrm{r}})$ for $k = -N/2, \ldots, N/2 - 1$.

Step 2. Scale the NUFFT output by the factors

$$
B(\rho\cos\theta, \rho\sin\theta) H(\rho) e^{-\imath 2\pi\rho\Delta_{\mathrm{r}}\eta_{\mathrm{r}}}
$$

from (10), and by the $1/\Delta_{\mathrm{r}}$ in (6). This yields the required $Z_\theta[k]$'s.

Step 3. Take the inverse K-point FFT of each Y_k set (for each θ) using (5). Discard all but the samples $n = 0, \ldots, N_{\mathrm{r}} - 1$. Check for residual imaginary part.

A minimally suitable choice for the PSF $h(r)$ would be $h(r) = \frac{1}{w}\mathrm{rect}\left(\frac{r}{w}\right)$ for which $H(f_{\mathrm{X}}) = \mathrm{sinc}(wf_{\mathrm{X}})$. This model accounts for the finite width of the detector elements. A typical choice for the basis function b is

$$
b(x, y) = \mathrm{rect}\left(\frac{x}{\Delta_1}\right) \mathrm{rect}\left(\frac{y}{\Delta_2}\right).
$$

B. Arc correction extension

The inverse FFT (5) yields uniformly-spaced radial samples. Typical PET systems having circular geometries acquire nonuniform radial samples. For conventional FBP reconstruction prior to ramp filtering one interpolates the nonuniform radial samples onto equally-spaced samples, often called *arc correction*. Such "preprocessing" interpolation is suboptimal for iterative reconstruction since it destroys the statistical independence of the measurements. It is preferable to build the nonuniform spacing into the reprojection method.

The min-max NUFFT interpolation method described in [11] is directly applicable to the case where (5) is replaced by nonuniform radial sampling.

C. Adjoint

The method described above is a linear operator and hence corresponds implicitly to some $(N_\theta \cdot N_{\mathrm{r}}) \times (N_1 \times N_2)$ matrix. Iterative algorithms usually also need the ability to compute matrix-vector multiplication by the transpose of that matrix, even though the matrix itself is not stored explicitly. It is straightforward to "reverse" (not invert!) the steps described above to develop an algorithm to perform multiplicaton by the transpose, corresponding to the adjoint of the forward operator, which is a form of backprojection.

IV. RESULTS

We evaluated the accuracy of the NUFFT-based reprojector using the Shepp-Logan digital phantom [2,55] with $N_1 \times N_2 = 128 \times 128$ pixels as shown in Fig. 1. We simulated a parallel-beam tomographic system with a sinogram

size of $N_\mathrm{r} = 160$ radial bins by $N_\theta = 192$ angles over $180°$, corresponding to CTI EXACT PET scanners. We included a rectangular detector response $h(r) = \mathrm{rect}(r)$ with width equal to the pixel size, partially representing the finite detector width in a PET system (rather than using overly idealized line integrals).

We computed forward projections of this object three ways: using Fourier-based reprojection with *exact* (to within double precision in Matlab) evaluation of the 2D FT (9), using Fourier-based reprojection with the 2D NUFFT approximation to (9) using min-max optimized Kaiser-Bessel interpolation with $J = 4$ and $K/N = 2$, and using a bilinear interpolation approximation to (9). Fig. 1 shows a representative example; the sinograms are visually indistinguishable. The maximum percent difference between the NUFFT method and the exact FT method, defined by

$$\frac{\max_{n,\theta} |y_\theta^{\mathrm{FT}}(n) - y_\theta^{\mathrm{NUFFT}}(n)|}{\max_{n,\theta} |y_\theta^{\mathrm{FT}}(n)|} \cdot 100\%,$$

is only 0.04%. By comparison, using conventional bilinear interpolation for the polar to cartesian conversion yielded maximum error of over 3%. The min-max NUFFT approach reduces the maximum error by two orders of magnitude for this choice of J.

Iterative algorithms also require the adjoint operator (backprojector). Fig. 2 compares the adjoint of the exact Fourier-based reprojector and the adjoint of the NUFFT-based reprojector (using the Kaiser-Bessel interpolator with $J = 4$ and $K/N = 2$) when applied to a ramp-filtered sinogram. Again the NUFFT approach agreed with the exact approach within 0.08%, which is certainly well below the noise levels in typical PET scans.

For a more systematic comparison, we compared the exact Fourier-reprojected sinograms to the the NUFFT-based sinograms for several values of the neighborhood size $J = J_1 = J_2$ and the FFT oversampling factor K/N. For simplicity we used *uniform scaling factors* for this study. For reasonable values of J and K/N the sinograms are indistinguishable when printed in grayscale or in profiles, so are not shown. Fig. 3 shows the tradeoff between computation time (using Matlab's `tic` command on a 1GHz Pentium III running Linux) and percent RMS difference between the exact approach and the NUFFT-based approach. We also examined the l_1 and l_∞ norm differences which showed identical trends. This figure shows that an oversampling factor of $K/N = 2$ provides a good tradeoff between accuracy and computation time for this geometry and computer. Using $J \approx 6$ with $K/N = 2$ seems to be a reasonable compromise. Using $J = 5$ and

$K/N = 2$, the NUFFT approach is over 500 times faster than the exact Fourier reprojector. In this case, precomputing the interpolation coefficients required less than 9 seconds and used about 17Mbyte of storage (with Matlab's double precision values). This precomputation depends only on the scanner geometry, and not the object, so needs only to be done once for a given tomographic system so its computation time is largely irrelevant.

Since iterative algorithms require repeated forward and backprojections, it is conceivable that even small errors in the reprojector could accumulate. We simulated noisy PET sinogram measurements from the phantom shown in Fig. 4. We ran 20 iterations of the conjugate gradient algorithm for a data-weighted least-squares cost function [13] with a standard quadratic first-order roughness penalty. We ran it twice; once with the exact Fourier-based reprojector, and once with the NUFFT approximation using $J = 5$ and $K/N = 2$ and the Kaiser-Bessel interpolator. Fig. 4 shows that the reconstructed images were visually indistinguishable. The maximum percent difference was less than 0.12% at the 20th iteration. So perhaps there is slight error accumulation with iteration, but it is negligible relative to Poisson noise.

The difference between the FBP image and the QPWLS-CG image is not so dramatic in this 2D example. The difference should be more significant in 3D acquisitions.

We have focused on comparing the NUFFT approximation to the sum (9) against exact evaluation by the discrete-space Fourier transform. This has allowed us to focus on the effects of the interpolation errors in the NUFFT approach. However, we must acknowledge that (5) is itself an approximation that in some sense "degrades" both the NUFFT and the DSFT relative to the *exact* formula (2). In the case of square pixels and a rectangular PSF $h(r)$ as we have used in these examples, it is possible to compute (2) exactly. Returning to the Shepp-Logan phantom, we computed the exact projection using (2) and (7) and compared it to the Fourier-based reprojector using the exact DSFT. The maximum percent difference of the sinograms was 0.74%. So this is the magnitude of the error introduced by the discretization (5). It must also be acknowledged that the series expansion (7) is an approximation in practice. It is quite plausible that the modeling error in that approximation will dominate the $\ll 1\%$ errors we have reported here for the NUFFT approach, so we conclude that the NUFFT approach with min-max interpolation is viable since the interpolation errors are smaller than the discretization errors inherent to and Fourier-based reprojector, which in turn are probably smaller than the object

discretization errors.

V. DISCUSSION

We have described a Fourier-based reprojection method using the NUFFT with min-max interpolation for the polar to Cartesian conversion in spatial frequency space. The method yields accuracies that are considerably improved over conventional bilinear interpolation. We have not yet compared to Kaiser-Bessel or gaussian interpolation in this context. We showed in [11] that the optimized min-max method (with optimized scaling factors) outperforms gaussian interpolation (even with numerically optimized width) in the 1D case by about an order of magnitude.

There are several limitations of Fourier-based reprojection that would need to be overcome before it would be widely used in iterative tomographic image reconstruction.

Due to interpolation errors, sinograms with slightly negative values may be produced, even for a nonnegative input image. In our implementation we simply truncate to zero any negative values (when the input image is nonnegative). Strictly speaking this nonlinearity could affect the convergence of some iterative algorithms, an issue that could be investigated further.

There is not an obvious approach to forming fan-beam projections, at least not without further interpolations that conceivably may degrade spatial resolution. An exception would be when the fan angle is small [56]. Perhaps a min-max approach could be found for the parallel-fan interpolation, perhaps by some change of variables. Thus the applicability to X-ray CT is an open question. Cone-beam CT is an additional challenge [36].

The Fourier approach appears unsuitable for SPECT since it cannot easily accommodate nonuniform attenuation and depth-dependent detector response. Perhaps some form of the frequency distance principle could overcome this limitation? Combining with fast rotation methods may be another avenue to explore [57].

The simplest version of the method is only suitable for shift-invariant radial blur, which is only an approximation to the PSF of PET systems. However, one could combine ideal "line integral" reprojection with a subsequent shift-variant radial blur operator to model effects such as crystal penetration partially. Such a factorized model would not include the depth-dependent effects that are particularly relevant when the object field of view approaches closely the detector ring, such as in some small-animal PET scanner designs.

The method is not ideally suited to "ordered-subsets" or block-iterative methods since the greatest efficiency comes from following the oversampled 2D FFT by calculation of *all* projection views. This would seem to limit the applicability to primarily the conjugate-gradient family of algorithms where ordered subsets are not needed.

Bronstein *et al.* have recently applied this algorithm to diffraction tomography [58].

VI. ACKNOWLEDGEMENT

REFERENCES

[1] S Basu and Y Bresler, "$O(n^2 \log_2 n)$ filtered backprojection reconstruction algorithm for tomography," *IEEE Tr. Im. Proc.*, vol. 9, no. 10, pp. 1760–73, Oct. 2000.

[2] A C Kak and M Slaney, *Principles of computerized tomographic imaging*, IEEE Press, New York, 1988.

[3] C R Crawford, "System for reprojecting images using transform techniques," 1986, US Patent 4,616,318. Filed 1983-6-7. Elscint.

[4] C R Crawford, J G Colsher, N J Pelc, and A H R Lonn, "High speed reprojection and its applications," in *Proc. SPIE 914, Med. Im. II: Im. Formation, Detection, Processing, and Interpretation*, 1988, pp. 311–8.

[5] C W Stearns, D A Chesler, and G L Brownell, "Three-dimensional image reconstruction in the Fourier domain," *IEEE Tr. Nuc. Sci.*, vol. 34, no. 1, pp. 374–8, Feb. 1987.

[6] C W Stearns, D A Chesler, and G L Brownell, "Accelerated image reconstruction for a cylindrical positron tomograph using Fourier domain methods," *IEEE Tr. Nuc. Sci.*, vol. 37, no. 2, pp. 773–7, Apr. 1990.

[7] F Natterer, *The mathematics of computerized tomography*, Teubner-Wiley, Stuttgart, 1986.

[8] J A Fessler and B P Sutton, "A min-max approach to the multidimensional nonuniform FFT: Application to tomographic image reconstruction," in *Proc. IEEE Intl. Conf. on Image Processing*, 2001, vol. 1, pp. 706–9.

[9] B P Sutton, J A Fessler, and D Noll, "A min-max approach to the nonuniform N-D FFT for rapid iterative reconstruction of MR images," in *Proc. Intl. Soc. Mag. Res. Med.*, 2001, p. 763.

[10] J A Fessler and Bradley P Sutton, "Tomographic image reconstruction using the nonuniform FFT," in *SIAM Conf. Imaging Sci.*, 2002, Invited presentation.

[11] J A Fessler and B P Sutton, "Nonuniform fast Fourier transforms using min-max interpolation," *IEEE Tr. Sig. Proc.*, vol. ?, 2001, Submitted to IEEE T-SP on 2001-12-19.

[12] A H Delaney and Y Bresler, "A fast and accurate Fourier algorithm for iterative parallel-beam tomography," *IEEE Tr. Im. Proc.*, vol. 5, no. 5, pp. 740–53, May 1996.

[13] J A Fessler, "Penalized weighted least-squares image reconstruction for positron emission tomography," *IEEE Tr. Med. Im.*, vol. 13, no. 2, pp. 290–300, June 1994.

[14] S Matej and R M Lewitt, "3-FRP: direct Fourier reconstruction with Fourier reprojection for fully 3-D PET," *IEEE Tr. Nuc. Sci.*, vol. 48, no. 4-2, pp. 1378–1385, Aug. 2001.

[15] S Matej, M E Daube-Witherspoon, and J S Karp, "Performance of 3D RAMLA with smooth basis functions on fully 3D PET data," in *f3d01*, 2001, pp. 193–6.

[16] J D O'Sullivan, "A fast sinc function gridding algorithm for Fourier inversion in computer tomography," *IEEE Tr. Med. Im.*, vol. 4, no. 4, pp. 200–207, Dec. 1985.

[17] J I Jackson, C H Meyer, D G Nishimura, and A Macovski, "Selection of a convolution function for Fourier inversion using gridding," *IEEE Tr. Med. Im.*, vol. 10, no. 3, pp. 473–8, Sept. 1991.

[18] R M Mersereau and A V oppenheim, "Digital reconstruction of multidimensional signals from their projections," *Proc. IEEE*, vol. 62, pp. 1319–38, 1974.

[19] R M Mersereau, "Recovering multidimensional signals from their projections," *Comp. Graphics and Im. Proc.*, vol. 1, pp. 179–85, 1974.

[20] R M Mersereau, "Direct Fourier transform techniques in 3-D image reconstruction," *Computers in Biology and Medicine*, vol. 6, pp. 247–58, 1976.

[21] H Stark, J W Woods, I Paul, and R Hingorani, "An investigation of computerized tomography by direct Fourier inversion and optimimum interpolation," *IEEE Tr. Biomed. Engin.*, vol. 28, no. 7, pp. 496–505, July 1981.

[22] H Stark, J W Woods, I Paul, and R Hingorani, "Direct Fourier reconstruction in computer tomography," *IEEE Tr. Acoust. Sp. Sig. Proc.*, vol. 29, no. 2, pp. 237–44, Apr. 1981.

[23] R M Lewitt, "Reconstruction algorithms: transform methods," *Proc. IEEE*, vol. 71, no. 3, pp. 390–408, Mar. 1983.

[24] N Niki, R T Mizutani, Y Takahasi, and T Inouye, "A high-speed computerized tomography image reconstruction using direct two-dimensional Fourier transform method," *Syst. Comput. Controls*, vol. 14, no. 3, pp. 56–65, 1983.

[25] F Natterer, "Fourier reconstruction in tomography," *Numerische Mathematik*, vol. 47, pp. 343–53, 1985.

[26] S X Pan and A C Kak, "A computational study of reconstruction algorithms for diffraction tomography: interpolation versus filtered backprojection," *IEEE Tr. Acoust. Sp. Sig. Proc.*, vol. 31, pp. 1263–75, 1983.

[27] H Peng and H Stark, "Direct Fourier reconstruction in fan-beam tomography," *IEEE Tr. Med. Im.*, vol. 6, no. 3, pp. 209, Sept. 1987.

[28] W Lawton, "A new polar Fourier transform for computer-aided tomography and spotlight synthetic aperture radar," *IEEE Tr. Acoust. Sp. Sig. Proc.*, vol. 36, no. 6, pp. 931–3, June 1988.

[29] S Matej and I Bajla, "A high-speed reconstruction from projections using direct Fourier method with optimized parameters-an experimental analysis," *IEEE Tr. Med. Im.*, vol. 9, no. 4, pp. 421–9, Dec. 1990.

[30] W K Cheung and R M Lewitt, "Modified Fourier reconstruction method using shifted transform samples," *Phys. Med. Biol.*, vol. 36, no. 2, pp. 269–77, Feb. 1991.

[31] M Magnusson, P-E Danielsson, and P Edholm, "Artefacts and remedies in direct Fourier tomographic reconstruction," in *Proc. IEEE Nuc. Sci. Symp. Med. Im. Conf.*, 1992, vol. 2, pp. 1138–40.

[32] M Tabei and M Ueda, "Backprojection by upsampled Fourier series expansion and interpolated FFT," *IEEE Tr. Im. Proc.*, vol. 1, no. 1, pp. 77–87, Jan. 1992.

[33] M Defrise, A Geissbuhler, and D W Townsend, "A performance study of 3D reconstruction algorithms for positron emission tomography," *Phys. Med. Biol.*, vol. 39, no. 3, pp. 305–20, Mar. 1994.

[34] P L Bellon and S Lanzavecchia, "A direct Fourier method (DFM) for X-ray tomographic reconstructions and the accurate simulation of sinograms," *Int. J. Bio-Med. Comput*, vol. 38, pp. 55–69, 1995.

[35] H Schomberg and J Timmer, "The gridding method for image reconstruction by Fourier transformation," *IEEE Tr. Med. Im.*, vol. 14, no. 3, pp. 596–607, Sept. 1995.

[36] N J Dusaussoy, "VOIR: a volumetric image reconstruction algorithm based on Fourier techniques for inversion of the 3-D Radon transform," *IEEE Tr. Im. Proc.*, vol. 5, no. 1, pp. 121–31, Jan. 1996.

[37] Salvatore Lanzavecchia and Pier Luigi Bellon, "Electron tomography in conical tilt geometry. The accuracy of a direct Fourier method (DFM) and the suppression of non-tomographic noise," *Ultramicroscopy*, vol. 63, no. 3-4, pp. 247–61, July 1996.

[38] Pier Luigi Bellon and Salvatore Lanzavecchia, "Fast direct Fourier methods, based on one- and two-pass coordinate transformations, yield accurate reconstructions of x-ray CT clinical images," *Phys. Med. Biol.*, vol. 42, no. 3, pp. 443–64, Mar. 1997.

[39] Hyeokho Choi and David C Munson, "Direct-Fourier reconstruction in tomography and synthetic aperture radar," *Intl. J. Imaging Sys. and Tech.*, vol. 9, no. 1, pp. 1–13, 1998.

[40] D Gottlieb, B Gustafsson, and P Forssen, "On the direct Fourier method for computer tomography," *IEEE Tr. Med. Im.*, vol. 19, no. 3, pp. 223–32, Mar. 2000.

[41] J Waldén, "Analysis of the direct Fourier method for computer tomography," *IEEE Tr. Med. Im.*, vol. 19, no. 3, pp. 211–22, Mar. 2000.

[42] D Potts and G Steidl, "New Fourier reconstruction algorithms for computerized tomography.," in *Proc. SPIE 4119, Wavelet Appl. in Signal and Image Proc. VIII*, 2000, pp. 13–23.

[43] Daniel Potts and Gabriele Steidl, "A new linogram algorithm for computerized tomography," *IMA J. Numer. Anal.*, vol. 21, no. 3, pp. 769–82, July 2001.

[44] G T Herman, D Roberts, and L Axel, "Fully three-dimensional reconstruction from data collected on concentric cubes in Fourier space: implementation and a sample application to MRI," *Phys. Med. Biol.*, vol. 37, no. 3, pp. 673–89, Mar. 1992.

[45] C H Meyer, B S Hu, D G Nishimura, and A Macovski, "Fast spiral coronary artery imaging," *Magnetic Resonance in Medicine*, vol. 28, no. 2, pp. 202–13, 1992.

[46] D Rosenfeld, "An optimal and efficient new gridding algorithm using singular value decomposition," *Magnetic Resonance in Medicine*, vol. 40, no. 1, pp. 14–23, July 1998.

[47] V Rasche, R Proksa, R Sinkus, P Bornert, and H Eggers, "Resampling of data between arbitrary grids using convolution interpolation," *IEEE Tr. Med. Im.*, vol. 18, no. 5, pp. 385–92, May 1999.

[48] H Sedarat and D G Nishimura, "On the optimality of the gridding reconstruction algorithm," *IEEE Tr. Med. Im.*, vol. 19, no. 4, pp. 306–17, Apr. 2000.

[49] F T A W Wajer, R Lethmate, J A C van Osch, D Graveron-Demilly, M Fuderer, and D van Ormondt, "Simple formula for the accuracy of gridding," in *Proc. Intl. Soc. Mag. Res. Med.*, 2001, p. 776.

[50] S Dunne, S Napel, and B Rutt, "Fast reprojection of volume data," in *Proc. of First Conf on Visualiztion in Biomedical Computing*, 1990, pp. 11–8.

[51] T Malzbender, "Fourier volume rendering," *ACM Trans. on Graphics*, vol. 12, no. 3, pp. 233–50, 1993.

[52] T Totsuka and M Levoy, "Frequency-domain volume rendering," in *Siggraph 93*, 1993, pp. 271–8.

[53] K Mueller and R Yagel, "On the use of graphics hardware to accelerate algebraic reconstruction methods," in *Proc. SPIE 3659, Phys. of Medical Imaging*, 1999, pp. 615–25.

[54] K Mueller and R Yagel, "Rapid 3-D cone-beam reconstruction with the simultaneous algebraic reconstruction technique (SART) using 2-D texture mapping hardware," *IEEE Tr. Med. Im.*, vol. 19, no. 12, pp. 1227–, Dec. 2000.

[55] L A Shepp and B F Logan, "The Fourier reconstruction of a head section," *IEEE Tr. Nuc. Sci.*, vol. 21, no. 3, pp. 21–43, June 1974.

[56] S Alliney, S Matej, and I Bajla, "On the possibility of direct Fourier reconstruction from divergent-beam projections," *IEEE Tr. Med. Im.*, vol. 12, no. 2, pp. 173–81, June 1993.

[57] R W Cox and Raoqiong Tong, "Two- and three-dimensional image rotation using the FFT," *IEEE Tr. Im. Proc.*, vol. 8, no. 9, pp. 1297–9, Sept. 1999.

[58] Michael Bronstein, Alexander Bronstein, and Michael Zibulevsky, "Iterative reconstruction in diffraction tomography using nonuniform fast Fourier transform," 2002.
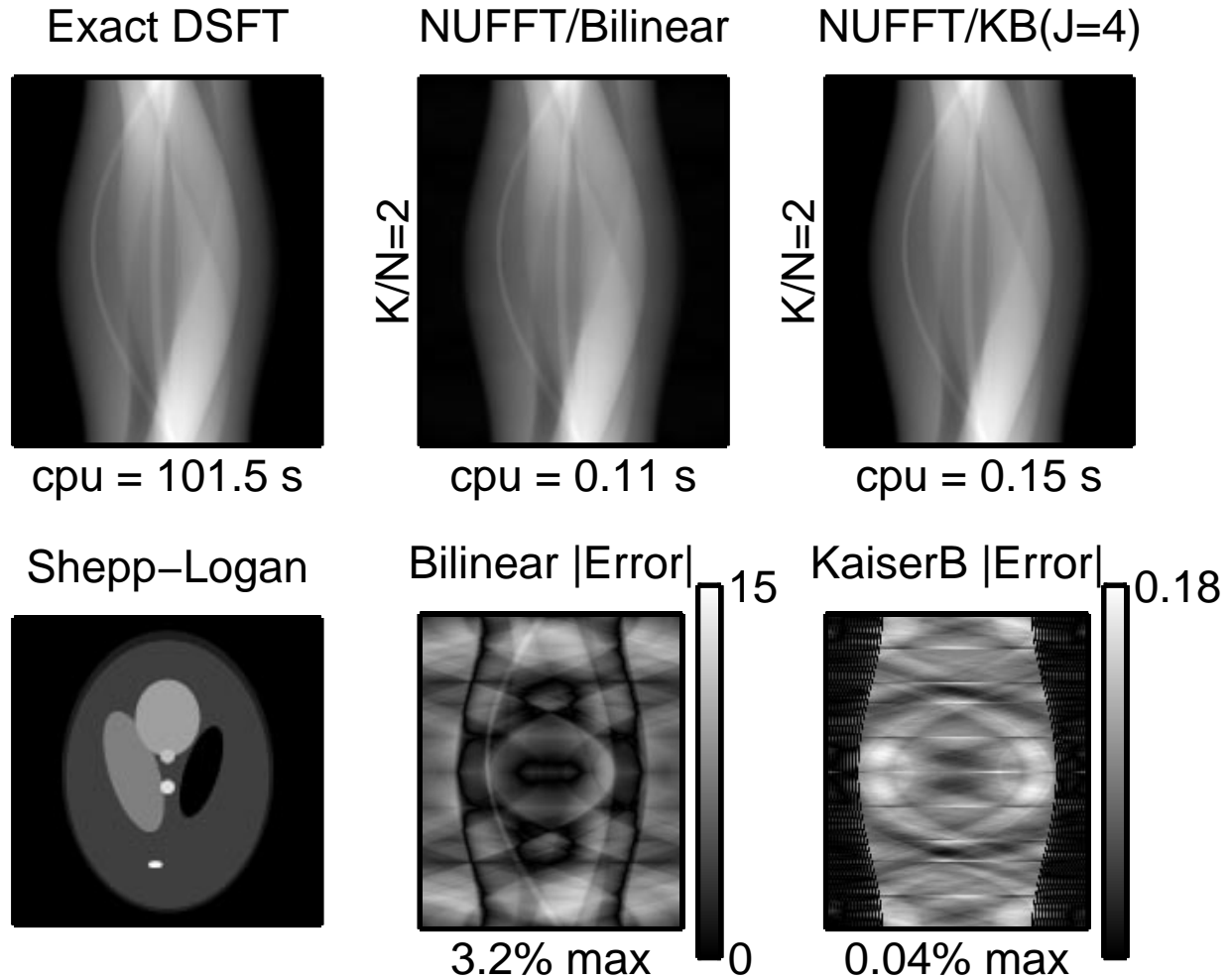
Figure 1: Shepp-Logan digital object and its sinograms computed by exact Fourier reprojection, Fourier reprojection with bilinear interpolation, and NUFFT reprojection with min-max interpolation. The scales on the error sinograms differ by two orders of magnitude.

Sinogram

Exact DSFT

NUFFT/KB

J=4, K/N=2

cpu = 144.0 s
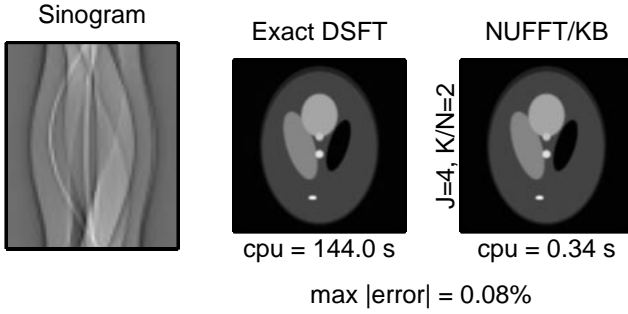
cpu = 0.34 s

max |error| = 0.08%

Figure 2: The adjoints of the exact FT-based reprojector and NUFFT-based reprojector yield very similar backprojector.
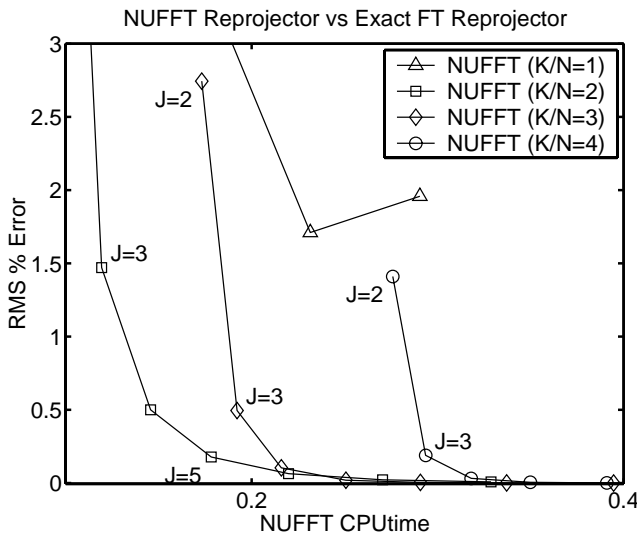

Figure 3: RMS error vs CPU time tradeoff for NUFFT-based reprojector with min-max interpolation and uniform scaling factors.

VII. APPENDIX: DISCRETIZING

Here are two other possible approaches to discretizing (3), neither of which seems preferable to (5).

A. *Even number of mid-point samples*

If we want an even number of samples when discretizing the integral (3), then we could use the midpoints between each integer by defining $Y_k = Y((k + 1/2)\delta)$. Using the natural spacing $\delta = 1/(N\Delta_\mathrm{r})$ yields:

$$
\begin{aligned}
y(n) &\approx \sum_{k=-N/2}^{N/2-1} \delta Y_k e^{\imath 2\pi[(k+1/2)\delta]\Delta_\mathrm{r} n} \\
&= \delta e^{\imath 2\pi(\delta/2)\Delta_\mathrm{r} n} \sum_{k=-N/2}^{N/2-1} Y_k e^{\imath 2\pi k\delta\Delta_\mathrm{r} n}
\end{aligned}
$$

$$
\approx \quad \frac{1}{\Delta_\mathrm{r}} e^{\imath \frac{2\pi}{N} n/2} \left[\frac{1}{N} \sum_{k=-N/2}^{N/2-1} Y_k e^{\imath 2\pi kn/N} \right] . \text{(11)}
$$

This is precisely the iFFT with a scale factor in front. However, this approach has the disadvantage that it never uses the DC sample location $Y(0)$, which will be exact in the NUFFT (with uniform scaling factors), but rather frequency locations nearby that will need to be interpolated generally. This might lead to DC inconsistencies from projection view to projection view. The complex exponential in front of the final sum in (11) seems a bit of a nuisance too; it may lead to larger than desirable imaginary components.

B. *Odd number of "integer" samples*

Instead we might prefer to use $Y_k = Y(k\delta)$, *i.e.*, samples at integer multiples of δ. To preserve symmetries so that $y(n)$ is "as close to real as possible" then we could use an odd number of samples in the discretization:

$$
\begin{aligned}
y(n) &\approx \sum_{k=-N/2}^{N/2} \delta Y_k e^{\imath 2\pi(k\delta)\Delta_\mathrm{r} n} \\
&= \frac{1}{\Delta_\mathrm{r}} \frac{1}{N} \sum_{k=-N/2}^{N/2} Y_k e^{\imath 2\pi kn/N}.
\end{aligned}
$$

This is not quite the iDFT we want since it has $N + 1$ points, which will be odd since we are assuming that N is even. However, $Y_{N/2} = Y^\star_{-N/2}$ due to the Hermitian symmetry of $Y(\cdot)$, so the $\pm N/2$ terms in the above sum are

$$
\begin{aligned}
&Y_{-N/2} e^{\imath 2\pi(-N/2)n/N} + Y_{N/2} e^{\imath 2\pi(N/2)n/N} \\
&= Y_{-N/2}(-1)^n + Y^\star_{-N/2}(-1)^n \\
&= \left[Y_{-N/2} + Y^\star_{-N/2}\right] e^{\imath 2\pi(-N/2)n/N}
\end{aligned}
$$

so

$$
y(n) \approx \frac{1}{\Delta_\mathrm{r}} \frac{1}{N} \sum_{k=-N/2}^{N/2-1} Z_k e^{\imath 2\pi kn/N},
$$

where

$$
Z_k = \\
\begin{cases} 2\,\mathrm{real}\left(Y_{-N/2}\right), & k = -N/2 \\ Y_k, & k = -N/2+1, \ldots, N/2-1. \end{cases}
$$

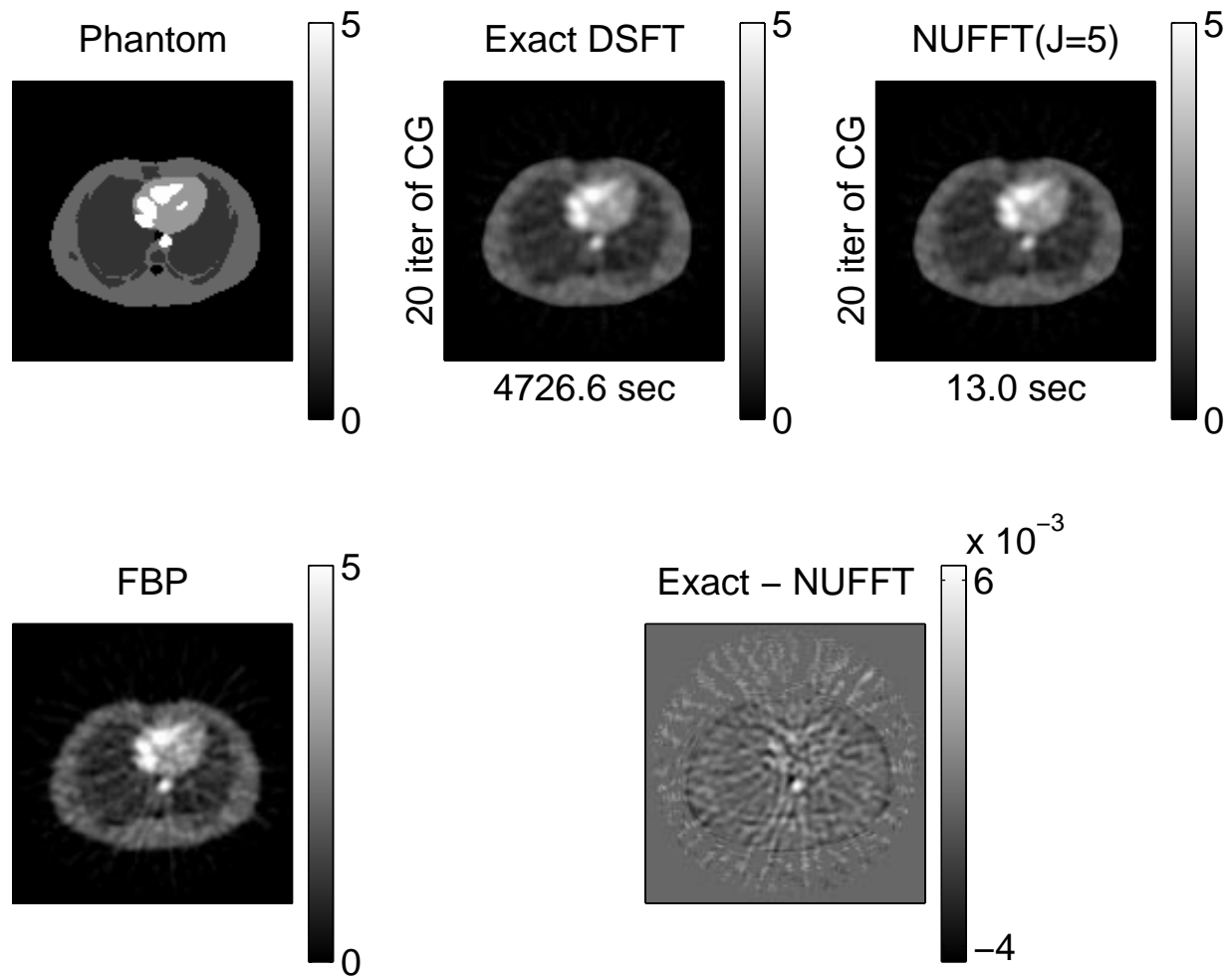Taking the real part is a nonlinear operation which I would prefer to avoid for iterative algorithms.

Figure 4: FBP and QPWLS-CG reconstructions of thorax phantom.